

Further lattice evidence for a large re-scaling of the Higgs condensate

P. Cea^{1,2}, M. Consoli³, L. Cosmai² and P. M. Stevenson⁴

¹ Dipartimento di Fisica, Università di Bari, via Amendola 173, I 70126 Bari, Italy

² INFN - Sezione di Bari, via Amendola 173, I 70126 Bari, Italy

³ INFN - Sezione di Catania, Corso Italia 57, I 95129 Catania, Italy

⁴ Bonner Laboratory, Physics Department, Rice University, Houston TX 77251, USA

Abstract

Using a high-statistics lattice simulation of the Ising limit of $(\lambda\Phi^4)_4$ theory, we have measured the susceptibility and propagator in the broken phase. We confirm our earlier finding of a discrepancy between the field re-scaling implied by the propagator data and that implied by the susceptibility. The discrepancy becomes *worse* as one goes closer to the continuum limit; thus, it cannot be explained by residual perturbative effects. The data are consistent with an unconventional description of symmetry breaking and “triviality” in which the re-scaling factor for the finite-momentum fluctuations tends to unity, but the re-scaling factor for the condensate becomes larger and larger as one approaches the continuum limit. In the Standard Model this changes the interpretation of the Fermi-constant scale and its relation to the Higgs mass.

1 Introduction

The well-established fact that the continuum limit of $(\lambda\Phi^4)_4$ theory is “trivial” [1–7] is traditionally interpreted using renormalized perturbation theory. In that picture, the ratio M_h^2/v_R^2 of the physical Higgs mass to the physical vacuum value v_R is proportional to the renormalized coupling λ_R and tends to zero as $1/\ln(\text{cutoff})$. Since v_R is fixed by the Fermi constant $v_R^2 \sim 1/(G_F\sqrt{2}) \sim (246\text{GeV})^2$, the physical Higgs mass is driven to zero in the continuum limit. To avoid that phenomenologically disastrous outcome one must invoke a finite cutoff Λ . A smaller cutoff value allows a larger Higgs mass, but the requirement that $\Lambda \geq 2M_h$ implies an upper bound on M_h [8].

In general, v_R differs from the bare “Higgs condensate” value measured on the lattice, $v_B \equiv \langle\Phi\rangle$. The two are related by a re-scaling factor Z :

$$v_R \equiv \frac{v_B}{\sqrt{Z}}. \quad (1)$$

In the conventional picture $Z = Z_{\text{prop}}$ where Z_{prop} is the wavefunction-renormalization constant for the propagator of the shifted field $\Phi(x) - \langle\Phi\rangle$. Due to ‘triviality,’ one expects $Z_{\text{prop}} \rightarrow 1$ in the continuum limit, in agreement with the perturbative prediction $Z_{\text{prop}} = 1 + \mathcal{O}(\lambda_R)$. Lattice data for the shifted-field propagator confirm that Z_{prop} is quite close to 1 [8].

However, a different interpretation of “triviality” has been proposed [9–11] in which there are two distinct “ Z ’s” in the broken-symmetry phase. The field $\Phi(x)$ must be divided into a finite-momentum piece and a zero-momentum (spacetime-constant) piece, φ . The former re-scales by the usual wavefunction-renormalization factor Z_{prop} , but the latter re-scales by a different factor, Z_φ . It is $Z = Z_\varphi$ that is needed in Eq. (1). Z_φ is determined by requiring the physical mass to match the second derivative of the effective potential with respect to the renormalized φ_R :

$$M_h^2 = \left. \frac{d^2 V_{\text{eff}}}{d\varphi_R^2} \right|_{\varphi_R=\pm v_R} = Z_\varphi \left. \frac{d^2 V_{\text{eff}}}{d\varphi_B^2} \right|_{\varphi_B=\pm v_B} = \frac{Z_\varphi}{\chi}, \quad (2)$$

where χ is the zero-momentum susceptibility.

Refs. [9–11] argue that in a “trivial” theory the effective potential should be effectively given by the sum of the classical potential and the zero-point energy of the shifted fluctuation field, which behaves as a free field. This leads to a V_{eff} that is extremely flat in terms of the bare field, implying a logarithmically divergent Z_φ of order $\ln(\Lambda/M_h)$. Therefore this interpretation of “triviality” predicts that $Z_{\text{prop}} \rightarrow 1$ and $Z_\varphi \rightarrow \infty$ in the infinite-cutoff limit.

A direct test of the “two Z ” picture was reported in our previous paper [12]. There we found a discrepancy between the Z_{prop} obtained from the propagator and the Z_φ obtained from $M_h^2\chi$. Absolutely no sign of such a discrepancy was found in the symmetric phase [12], as expected. Here we report a substantially refined calculation; it involves larger lattices and a tenfold increase in statistics. Our previous result is confirmed.

2 The lattice simulation

The one-component $(\lambda\Phi^4)_4$ theory

$$S = \sum_x \left[\frac{1}{2} \sum_{\mu} (\Phi(x + \hat{e}_{\mu}) - \Phi(x))^2 + \frac{r_0}{2} \Phi^2(x) + \frac{\lambda_0}{4} \Phi^4(x) \right] \quad (3)$$

becomes in the Ising limit

$$S_{\text{Ising}} = -\kappa \sum_x \sum_{\mu} [\phi(x + \hat{e}_{\mu})\phi(x) + \phi(x - \hat{e}_{\mu})\phi(x)] \quad (4)$$

with $\Phi(x) = \sqrt{2\kappa}\phi(x)$ and where $\phi(x)$ takes only the values $+1$ or -1 .

We performed Monte-Carlo simulations of this Ising action using the Swendsen-Wang [13] cluster algorithm. Statistical errors can be estimated through a direct evaluation of the integrated autocorrelation time [14], or by using the “blocking” [15] or the “grouped jackknife” [16] algorithms. We have checked that applying these three different methods we get consistent results.

We have measured the following lattice observables:

(i) the bare magnetization, $v_B = \langle |\Phi| \rangle$, where $\Phi \equiv \sum_x \Phi(x)/L^4$ is the average field for each lattice configuration,

(ii) the zero-momentum susceptibility

$$\chi = L^4 [\langle |\Phi|^2 \rangle - \langle |\Phi| \rangle^2], \quad (5)$$

(iii) the shifted-field propagator

$$G(p) = \left\langle \sum_x \exp(ipx) (\Phi(x) - v_B) (\Phi(0) - v_B) \right\rangle, \quad (6)$$

where $p_{\mu} = \frac{2\pi}{L} n_{\mu}$ with n_{μ} being a vector with integer-valued components, not all zero. We shall compare the lattice data for $G(p)$ to the 2-parameter formula

$$G_{\text{fit}}(p) = \frac{Z_{\text{prop}}}{\hat{p}^2 + m_{\text{latt}}^2}, \quad (7)$$

where m_{latt} is the mass in lattice units and $\hat{p}_{\mu} = 2 \sin \frac{p_{\mu}}{2}$. If “triviality” is true, then this form should give a better and better description of the lattice data as we approach the continuum limit; also, Z_{prop} should tend to unity.

Another way to determine the mass is to use the method of “time-slice” variables described in ref.[17] (see also [21] pp. 56). To this end let us consider a lattice with 3-dimension L^3 and temporal dimension L_t and the two-point correlator

$$C_1(t, 0; \mathbf{k}) \equiv \langle S_c(t; \mathbf{k}) S_c(0; \mathbf{k}) + S_s(t; \mathbf{k}) S_s(0; \mathbf{k}) \rangle_{\text{conn}}, \quad (8)$$

where

$$S_c(t; \mathbf{k}) \equiv \frac{1}{L^3} \sum_{\mathbf{x}} \phi(\mathbf{x}, t) \cos(\mathbf{k} \cdot \mathbf{x}), \quad (9)$$

$$S_s(t; \mathbf{k}) \equiv \frac{1}{L^3} \sum_{\mathbf{x}} \phi(\mathbf{x}, t) \sin(\mathbf{k} \cdot \mathbf{x}). \quad (10)$$

Here, t is the Euclidean time; \mathbf{x} is the spatial part of the site 4-vector x^μ ; \mathbf{k} is the lattice momentum $\mathbf{k} = (2\pi/L)(n_x, n_y, n_z)$, with (n_x, n_y, n_z) non-negative integers; and $\langle \dots \rangle_{\text{conn}}$ denotes the connected expectation value with respect to the lattice action, Eq. (4). In this way, parameterizing the correlator C_1 in terms of the energy ω_k as

$$C_1(t, 0; \mathbf{k}) = A [\exp(-\omega_k t) + \exp(-\omega_k(L_t - t))], \quad (11)$$

the mass can be determined through the lattice dispersion relation

$$m_{\text{TS}}^2(\mathbf{k}) = 2(\cosh \omega_k - 1) - 2 \sum_{\mu=1}^3 (1 - \cos k_\mu). \quad (12)$$

In a free-field theory m_{TS} is independent of \mathbf{k} and coincides with m_{latt} from Eq. (7).

3 Numerical results: symmetric phase

As a check of our simulations we started our analysis at $\kappa = 0.0740$ in the symmetric phase, where high-statistics results by Montvay and Weisz [17] are available. In Fig. 1 we report the data for the scalar propagator suitably re-scaled in order to show the very good quality of the fit to Eq. (7). The 2-parameter fit gives $m_{\text{latt}} = 0.2141(28)$ and $Z_{\text{prop}} = 0.9682(23)$. The value at zero-momentum is defined as $Z_\varphi \equiv m_{\text{latt}}^2 \chi = 0.9702(91)$. Notice the perfect agreement between Z_φ and Z_{prop} .

In Fig. 2 we show the values of the time-slice mass Eq. (12) at several values of the 3-momentum and the corresponding result of Ref. [17]. The shaded area corresponds to the value $m_{\text{latt}} = 0.2141(28)$ obtained from the fit to the propagator data. We see that m_{TS} is indeed independent of \mathbf{k} and agrees well with m_{latt} .

Thus, our analysis of the symmetric phase is in good agreement with Ref. [17] and shows the expected “trivial” behaviour. Note that our result for $Z_{\text{prop}} \simeq Z_\varphi$ is in excellent agreement with the 1-loop renormalization group prediction $Z_{\text{pert}} = 0.97(1)$ [5].

4 Numerical results: broken phase

We now choose for κ three successive values, $\kappa = 0.076, 0.07512, 0.07504$, lying just above the critical $\kappa_c \simeq 0.0748$ [17]. Thus, we are in the broken phase and approaching the continuum limit where the correlation length ξ becomes much larger than the lattice spacing.

We used lattice sizes L^4 with $L = 20, 32, 32$, respectively. This should ensure that finite-size effects are sufficiently under control, since in all cases $L/\xi > 5$ [17, 18]. Finite-volume tunneling effects [19, 20] should also be negligible, as we explain in the appendix. Finally, we also repeated the measurements for $\kappa = 0.076$ on an $L = 32$ lattice (with less statistics) to confirm directly the absence of finite-size effects in this case. After discarding 10K sweeps for thermalization, we have performed 500K sweeps (ten times more than in our earlier calculation [12]); the observables were measured every 5 sweeps. Our results for the magnetization and the susceptibility are reported in Table 1. We note that at $\kappa = 0.076$ our values are in excellent agreement with the corresponding results of Jansen *et al* [19].

The data for the re-scaled propagator are reported in Figs. 3–5. Unlike Fig. 1, the fit to Eq. (7), though excellent at higher momenta, does not reproduce the lattice data down to zero-momentum. Therefore, in the broken phase, a meaningful determination of Z_{prop} and m_{latt} requires excluding the lowest-momentum points from the fit. Fig. 6 shows how the chi-squared per d.o.f. of the fit improves, and the fitted value of m_{latt} stabilizes, as low-momentum points are excluded from the fit. Our numbers for m_{latt} and Z_{prop} are reported in Table 2. Z_{prop} is indicated in Figs. 3–5 by a dashed line.

The fitted Z_{prop} is slightly less than one. This fact is attributable to residual interactions since we are not exactly at the continuum limit, so that the theory is not yet completely “trivial.” This explanation is reasonable since we see a tendency for Z_{prop} to approach unity as we get closer to the continuum limit. Moreover, we find good agreement between our result, $Z_{\text{prop}} = 0.9321(44)$, and the Lüscher-Weisz perturbative prediction $Z_{\text{pert}} = 0.929(14)$ [5] at $\kappa = 0.0760$. The comparison $Z_{\text{prop}} = 0.9566(13)$ with $Z_{\text{pert}} = 0.940(12)$ at $\kappa = 0.07504$ is also fairly good.

The quantity Z_φ is obtained from the product $m_{\text{latt}}^2 \chi$ and is shown in Figs. 3–5, as a point at $\hat{p} = 0$. According to conventional ideas Z_φ should be *the same* as the wavefunction-renormalization constant, Z_{prop} , but clearly it is significantly larger. Note that there was no such discrepancy in Fig. 1 for the symmetric phase.

Our data show that the discrepancy gets *worse* as we approach the critical κ . Fig. 7 shows that Z_φ grows rapidly as one approaches the continuum limit (where $m_{\text{latt}} \rightarrow 0$). Thus, the effect cannot be explained by residual perturbative $\mathcal{O}(\lambda_R)$ effects that might cause $G(p)$ to deviate from the form in (7); such effects die out in the continuum limit, according to “triviality.”

The results accord well with the “two Z ” picture in which, as we approach the continuum limit, we expect to see the zero-momentum point, $Z_\varphi \equiv m_{\text{latt}}^2 \chi$, become higher and higher. In

the continuum limit the effect should be confined to the zero-momentum point, but it seems that, away from the continuum limit, the effect “spills over” into the very low momentum modes. This “spillover” would explain why the propagator deviates from free-field form at low \hat{p} , necessitating the exclusion of the lowest few \hat{p} points to get a good fit to (7). As we approach the continuum theory the deviation from the $Z_{\text{prop}}/(\hat{p}^2 + m_{\text{latt}}^2)$ form should become concentrated in a smaller and smaller range of \hat{p} , but with a larger and larger spike at $\hat{p} = 0$. In this limit the shape should become a discontinuous function that is infinite at $\hat{p} = 0$ and equal to 1 for all non-zero \hat{p} . The sequence of pictures in Figs. 3—5 is quite consistent with this expectation.

The time-slice mass $m_{\text{TS}}(\mathbf{k})$ also shows distinctive behaviour at low momentum, as seen in Fig. 8 for $\kappa = 0.076$. Except at low momentum the time-slice mass agrees well with m_{latt} . However, the time-slice mass at zero momentum, $m_{\text{TS}}(0)$, is very significantly smaller than m_{latt} (see Table 3). At $\kappa = 0.076$ our result for $m_{\text{TS}}(0)$ is in very good agreement with the corresponding result in Ref. [19]. The ratio $\frac{m_{\text{TS}}(0)}{m_{\text{latt}}}$ is shown in Fig. 9 as a function of m_{latt} . The trend is inverse to that in Fig. 7 for Z_{φ} .

Our interpretation of the data regards m_{latt} as the true particle mass and views $m_{\text{TS}}(0)$ as a symptom of the distinct dynamics of the zero-momentum mode. An alternative interpretation might be to regard $m_{\text{TS}}(0)$ as the true mass. However, we see two serious objections to that interpretation. Firstly, it would entail another “ Z ” factor, $Z_0 \equiv \chi m_{\text{TS}}(0)^2$, which turns out to be roughly 0.88 in all three cases. This Z_0 , unlike our Z_{prop} , would not agree well with the Lüscher and Weisz predictions. (In fact such a discrepancy in the $\kappa = 0.076$ case was noted by Jansen *et al* [19].) Secondly, if $m_{\text{TS}}(\mathbf{k})$ depends sensitively on \mathbf{k} , as it does near $\mathbf{k} = 0$, then the dispersion relation is not well approximated by the (lattice version of the) usual form $\omega_{\mathbf{k}} = \sqrt{\mathbf{k}^2 + \text{const.}}$; in that case the very notion of “mass” becomes problematic. At larger \mathbf{k} , where $m_{\text{TS}}(\mathbf{k})$ does become insensitive to \mathbf{k} , it agrees well with m_{latt} .

5 Conclusions

Our data clearly reveal unconventional behaviour at and near zero momentum in the broken phase. Well away from zero momentum the propagator data fit the “trivial” form $Z_{\text{prop}}/(\hat{p}^2 + m_{\text{latt}}^2)$, with Z_{prop} in accord with perturbative predictions [5]. However, the data deviate from this form at very low momentum, presaging an even more dramatic difference between Z_{prop} and $Z_{\varphi} \equiv m_{\text{latt}}^2 \chi$, where χ is the zero-momentum susceptibility. This difference gets rapidly *larger* as one gets closer to the continuum limit, $m_{\text{latt}} \rightarrow 0$; see Fig. 7. Because of this fact it is not possible to explain the effect in terms of residual perturbative interactions (even if one were to use a different value of the mass); perturbative effects should die out as one approaches the continuum limit, according to “triviality.” Finite-volume effects, including tunneling, should be negligible (see appendix). We note that at $\kappa = 0.076$, $L = 20$ our measurements are in complete agreement with Jansen *et al* [19] wherever a direct comparison is possible.

Our results are consistent with the unconventional picture of “triviality” and spontaneous symmetry breaking of refs. [9–11] in which Z_φ diverges logarithmically, while $Z_{\text{prop}} \rightarrow 1$ in the continuum limit. In this picture the Higgs mass M_h can remain finite in units of the Fermi-constant scale v_R , even though the ratio M_h/v_B goes to zero. The Higgs mass is then a genuine collective effect and M_h^2 is *not* proportional to the renormalized self-interaction strength. If so, then the whole subject of Higgs mass limits is affected. In view of the importance of the issue, both for theory and phenomenology, we hope and expect that our lattice results will be checked (and/or challenged) by other groups.

Acknowledgements We thank K. Jansen and J. Jersák for useful discussions and correspondence concerning the results of Refs. [19, 20].

This work was supported in part by the U.S. Department of Energy under Grant No. DE-FG05-92ER41031 and in part by the Istituto Nazionale di Fisica Nucleare.

Appendix: Tunneling effects

In this appendix we argue that tunneling effects are negligible in our data. Finite-volume tunneling effects in the Ising model have been studied very thoroughly by Jansen *et al* [19, 20]. In finite volume there is mixing between the $+v$ and $-v$ ‘ground states’ and the true ground state is the symmetric combination with energy $E_{0s} \equiv 0$. The antisymmetric combination is slightly higher in energy by an amount E_{0a} which depends on the lattice size L :

$$E_{0a} \approx CL^{1/2} \exp(-\sigma L^3). \quad (13)$$

This formula comes from a semiclassical instanton-type calculation, which also yields theoretical formulas for C and σ (Ref. [19], Sect. 4.3). For the case $\kappa = 0.076$, Jansen *et al* also measured E_{0a} on small lattices ($L \leq 10$) [20] and obtained values $\sigma = 0.00358(2)$, $C = 0.101$ that agree well with their theoretical formulas. Using their results we can estimate E_{0a} in our three cases ($\kappa = 0.076, 0.07512, 0.07504$ with $L = 20, 32, 32$, respectively). We find $E_{0a} = 2 \times 10^{-13}$, 3×10^{-8} , and 10^{-5} , respectively.

For the first excited state (in the zero 3-momentum sector) there are also two nearly degenerate states, E_{1s} and E_{1a} . The difference $E_{1a} - E_{1s}$ is considerably larger than E_{0a} . Ref. [20]’s data for $\kappa = 0.076$ shows that the ratio of $E_{1a} - E_{1s}$ to E_{0a} is around 6 for $L = 8$ and around 4 for $L = 10$. It therefore seems reasonable to assume that, for larger lattices, $E_{1a} - E_{1s}$ is not more than 4 times E_{0a} . (For $\kappa = 0.076, L = 20$ this implies $E_{1a} - E_{1s} \sim 10^{-12}$, so we are fully justified in averaging Ref. [19]’s results $E_{1s} = 0.3914(12)$ and $E_{1a} = 0.3909(14)$ in order to compare with our $m_{TS}(0)$ result in Table 3.)

Tunneling effects lead to a modification of the formulas for χ and the two-point correlator

C_1 . However, the effect of these modifications is tiny in our cases. When expanded for small E_{0a} , the non-trivial factor involved in χ (see Ref. [19], Eq. (24)) is seen to differ from unity only by an amount of order $E_{0a}^2 T^2$, where T is the lattice's temporal size. (There is a not-immediately-obvious cancellation of the terms linear in E_{0a} .) This difference from unity is tiny (10^{-23} , 10^{-12} , 10^{-7} , in our three cases). Therefore we believe that tunneling effects are too small to show up in our data.

References

- [1] M. Aizenman, Phys. Rev. Lett. **47**, 1 (1981).
- [2] J. Fröhlich, Nucl. Phys. **B200**(FS4), 281 (1982).
- [3] A. Sokal, Ann. Inst. H. Poincaré, **37**, 317 (1982).
- [4] K. G. Wilson and J. Kogut, Phys. Rep. **C12**, 75 (1974); G. A. Baker and J. M. Kincaid, Phys. Rev. Lett. **42**, 1431 (1979); B. Freedman, P. Smolensky and D. Weingarten, Phys. Lett. **B113**, 481 (1982); D. J. E. Callaway and R. Petronzio, Nucl. Phys. **B240**, 577 (1984); I. A. Fox and I. G. Halliday, Phys. Lett. **B 159**, 148 (1985); C. B. Lang, Nucl. Phys. **B 265**, 630 (1986).
- [5] M. Lüscher and P. Weisz, Nucl. Phys. **B 290**, 25 (1987); ibidem **B295**, 65 (1988).
- [6] J. Glimm and A. Jaffe, *Quantum Physics: A Functional Integral Point of View* (Springer, New York, 1981, 2nd Ed. 1987).
- [7] R. Fernández, J. Fröhlich, and A. D. Sokal, *Random Walks, Critical Phenomena, and Triviality in Quantum Field Theory* (Springer-Verlag, Berlin, 1992).
- [8] For a complete review and extensive reference to the original papers see, C. B. Lang, *Computer Stochastics in Scalar Quantum Field Theory*, in Stochastic Analysis and Application in Physics, Proc. of the NATO ASI, Funchal, Madeira, Aug. 1993, ed. L. Streit, Kluwer Acad. Publishers, Dordrecht 1994.
- [9] M. Consoli and P. M. Stevenson, Zeit. Phys. **C63**, 427 (1994).
- [10] M. Consoli and P. M. Stevenson, hep-ph/9407334.
- [11] M. Consoli and P. M. Stevenson, Phys. Lett. **B391**, 144 (1997).
- [12] P. Cea, M. Consoli and L. Cosmai, Mod. Phys. Lett. **A13**, 2361 (1998).
- [13] R. H. Swendsen and J.-S. Wang, Phys. Rev. Lett. **58**, 86 (1987).
- [14] N. Madras and A. D. Sokal, J. Stat. Phys. **50**, 109 (1988).

- [15] C. Whitmer, Phys. Rev. **D29**, 306 (1984); H. Flyvbjerg and H. G. Petersen, J. Chem. Phys. **91**, 461 (1989).
- [16] B. Efron, *Jackknife, the Bootstrap and Other Resampling Plans*, (SIAM Press, Philadelphia, 1982); B. A. Berg and A. H. Billoire, Phys. Rev. **D40**, 550 (1989).
- [17] I. Montvay and P. Weisz, Nucl. Phys. **B290**, 327 (1987).
- [18] M. Lüscher, Comm. Math. Phys. **104**, 177 (1986).
- [19] K. Jansen, I. Montvay, G. Münster, T. Trappenberg and U. Wolff, Nucl. Phys. **B322**, 698 (1989).
- [20] K. Jansen, J. Jersák, I. Montvay, G. Münster, T. Trappenberg and U. Wolff, Phys. Lett. **B213**, 203 (1988).
- [21] I. Montvay and G. Münster, *Quantum Fields on a Lattice*, Cambridge University Press, 1994.

Ref.	L_{size}	# sweeps	κ	$\frac{v_B}{\sqrt{2\kappa}}$	$\frac{\chi}{2\kappa}$
Our data	20^4	5×10^5	0.076	0.3015(1)	37.71(22)
Ref. [19]	20^4	7.5×10^6	0.076	0.30158(2)	37.85(6)
Our data	32^4	2.5×10^5	0.076	0.3015(1)	37.70(31)
Our data	32^4	4×10^5	0.07512	0.1617(1)	193.1 ± 1.7
Our data	32^4	5×10^5	0.07504	0.13822(12)	293.38 ± 2.86

Table 1: The lattice data for the magnetization and the susceptibility.

L_{size}	# sweeps	κ	m_{latt}	Z_{prop}	Z_φ
20^4	5×10^5	0.076	0.42865(456)	0.9321(44)	1.0531(232)
32^4	2.5×10^5	0.076	0.42836(500)	0.9312(27)	1.0516(260)
32^4	4×10^5	0.07512	0.20623(409)	0.9551(21)	1.2340(502)
32^4	5×10^5	0.07504	0.17229(336)	0.9566(13)	1.307(52)

Table 2: Our values for m_{latt} and Z_{prop} as obtained from a fit to the lattice data for the propagator (see Figs.3–5). We also report $Z_\varphi \equiv m_{\text{latt}}^2 \chi$ where the χ 's are given in Table 1.

Ref.	L_{size}	# sweeps	κ	$m_{\text{TS}}(0)$	m_{latt}
Our data	20^4	5×10^5	0.076	0.388(10)	0.42865(456)
Ref. [19]	20^4	7.5×10^6	0.076	0.3912(12)	–
Our data	32^4	4×10^5	0.07512	0.1737(24)	0.20623(409)
Our data	32^4	5×10^5	0.07504	0.1419(17)	0.17229(336)

Table 3: The lattice data for the zero-momentum time-slice mass compared with the mass from the finite-momentum propagator. The result of Ref. [19] is an average of the two values E_{1s} and E_{1a} reported in their Table 4.

FIGURE CAPTIONS

- Figure 1. The lattice data for the re-scaled propagator at $\kappa = 0.0740$ in the symmetric phase. The zero-momentum full point is defined as $Z_\varphi = m_{\text{latt}}^2 \chi$. The dashed line indicates the value of Z_{prop} .
- Figure 2. The data for the time-slice mass Eq.(12) at different values of the 3-momentum. The shaded area represents the value $m_{\text{latt}} = 0.2141(28)$ obtained from the fit of the propagator data. The black square is the result of Ref. [17].
- Figure 3. The lattice data for the re-scaled propagator at $\kappa = 0.076$. The zero-momentum full point is defined as $Z_\varphi = m_{\text{latt}}^2 \chi$. The very low momentum region is shown in the inset. The dashed line indicates the value of Z_{prop} .
- Figure 4. The same as in Fig. 3 at $\kappa = 0.07512$.
- Figure 5. The same as in Fig. 3 at $\kappa = 0.07504$.
- Figure 6. The values of the reduced chi-square and of the fitted m_{latt} as a function of the number of low-momentum points excluded from the fit to Eq.(7).
- Figure 7. The two re-scaling factors Z_{prop} and Z_φ as a function of m_{latt} . (The continuum limit corresponds to $m_{\text{latt}} \rightarrow 0$.)
- Figure 8. The time-slice mass $m_{\text{TS}}(\mathbf{k})$ for several values of the spatial momentum. The black square at zero momentum is the result of Ref. [19]. The shaded area represents the value $m_{\text{latt}} = 0.42865(456)$ obtained from the fit to the propagator data.
- Figure 9. The ratio $\frac{m_{\text{TS}}(0)}{m_{\text{latt}}}$ as a function of m_{latt} .

$20^4, \kappa=0.0740$
(215K configs., 43K meas.)

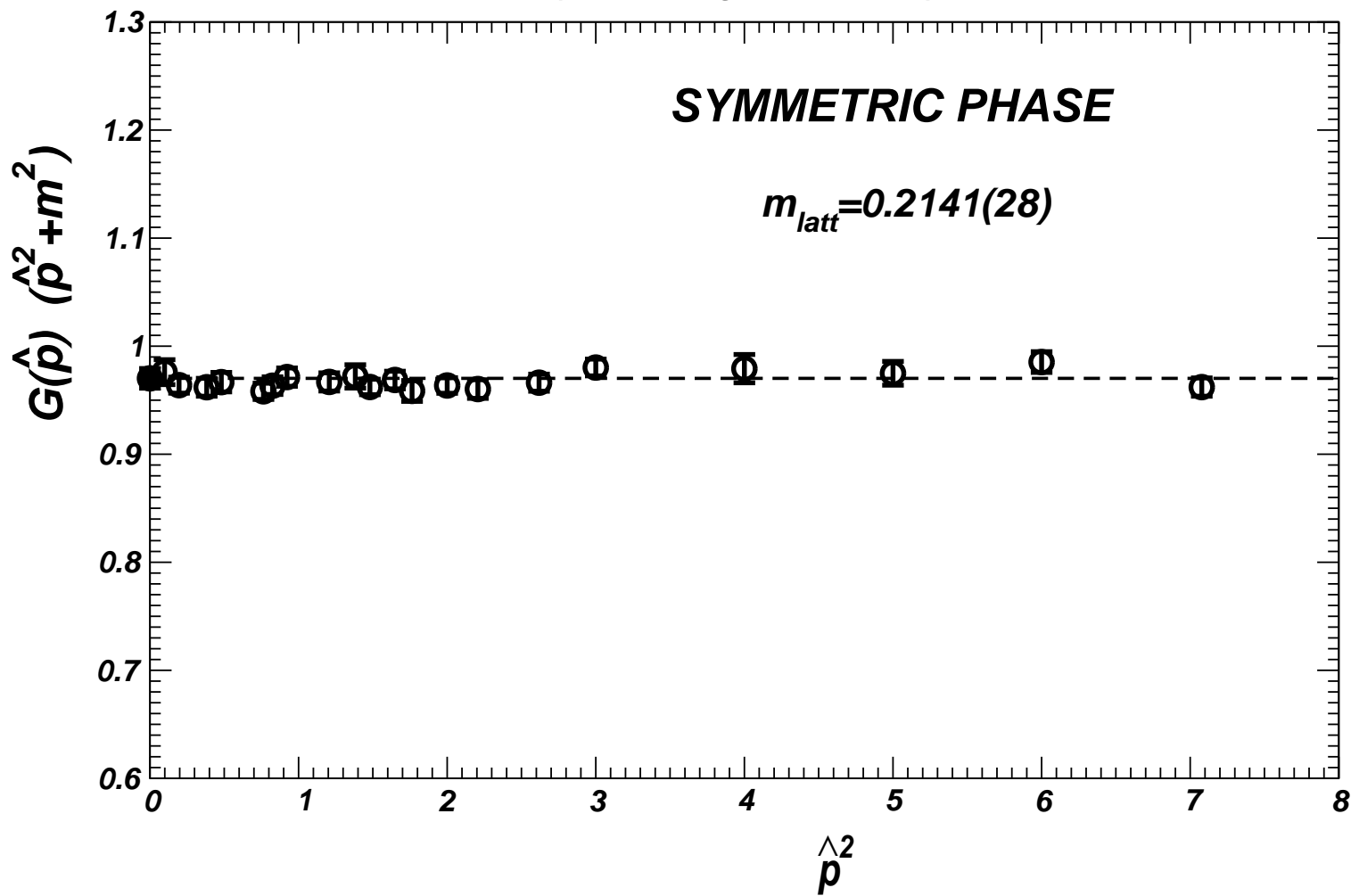


FIGURE 1

20^4 lattice
(215K configs. , 43K meas.)

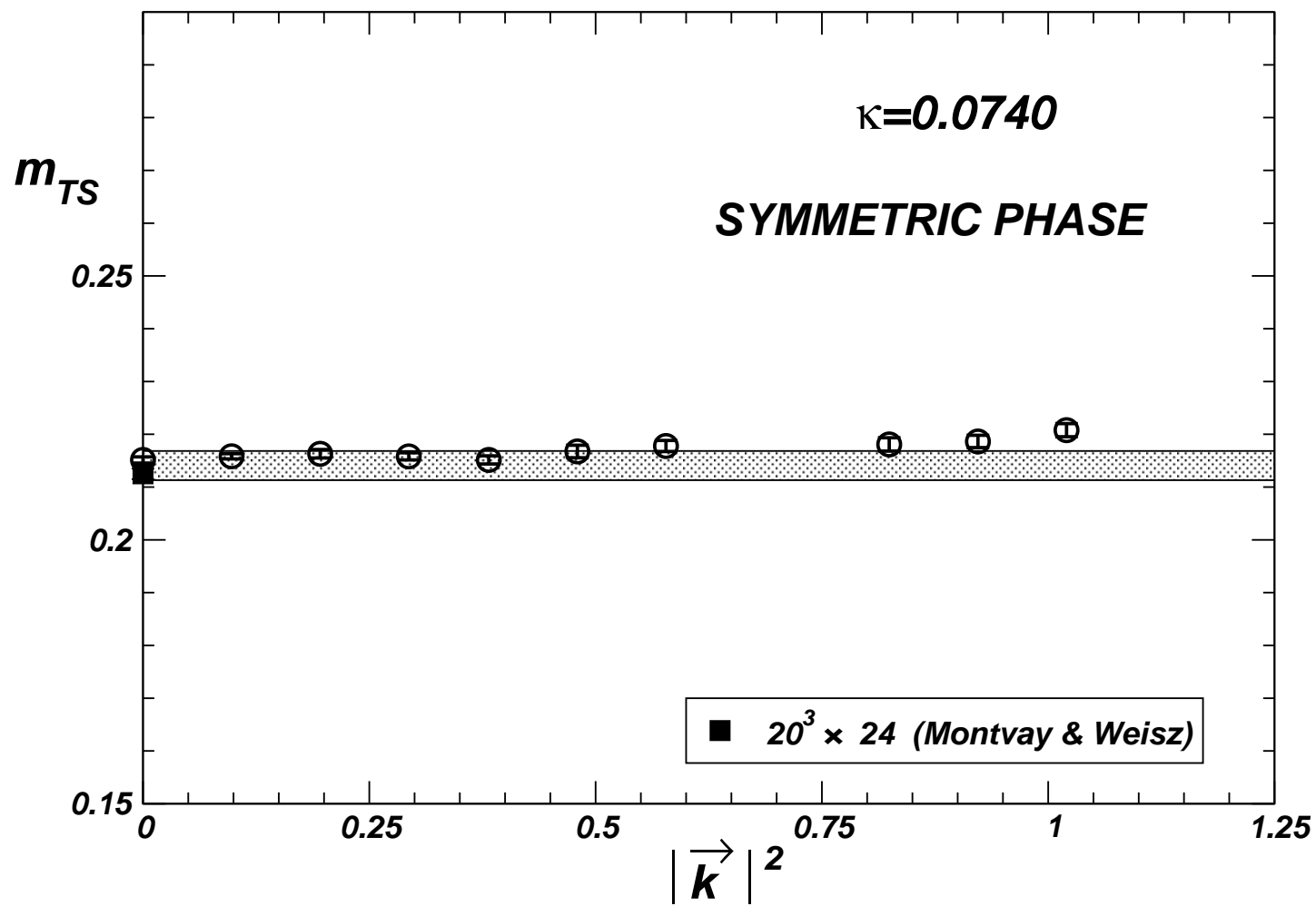


FIGURE 2

$20^4, \kappa=0.0760$
(500K configs., 100K meas.)

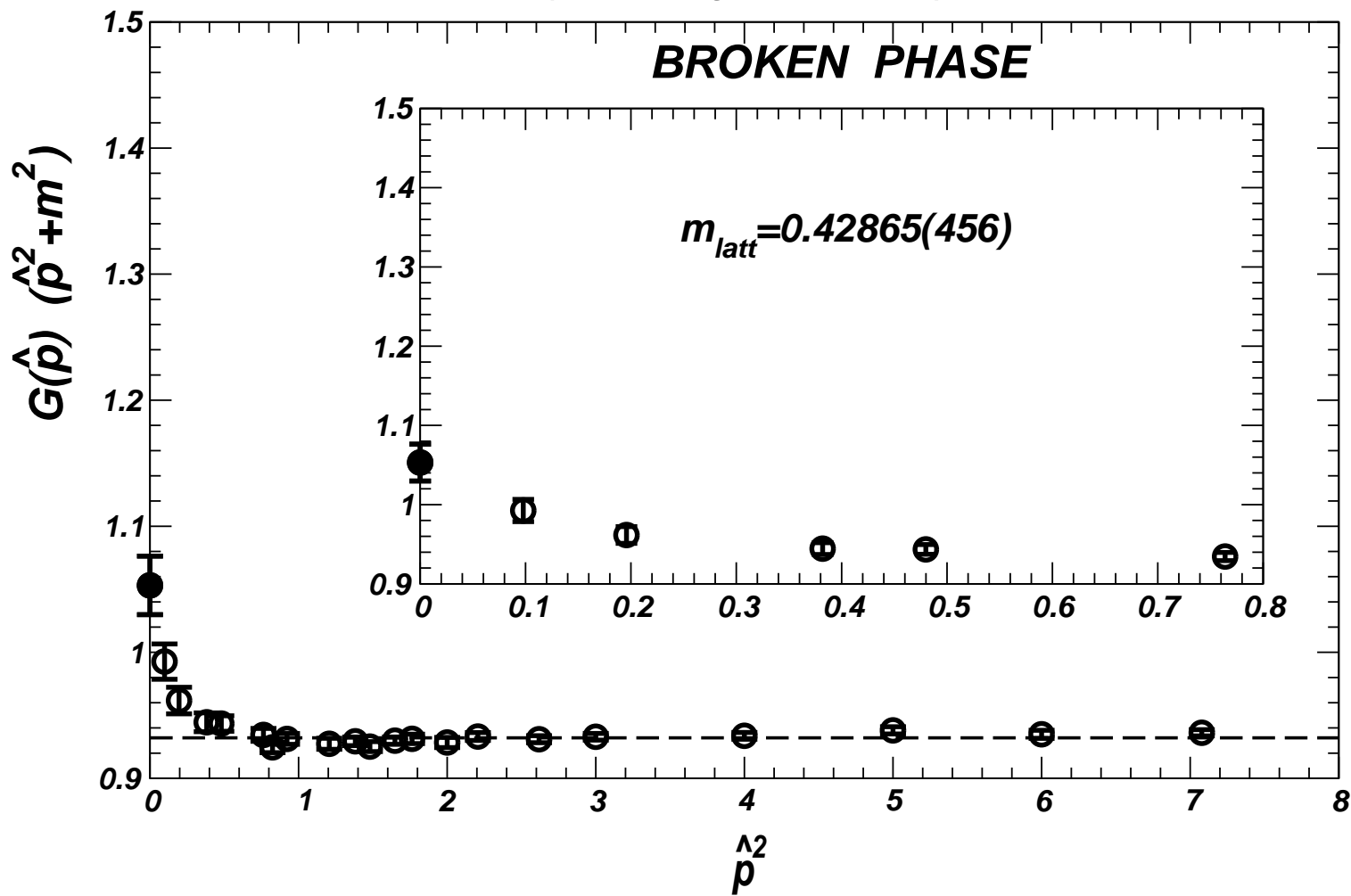


FIGURE 3

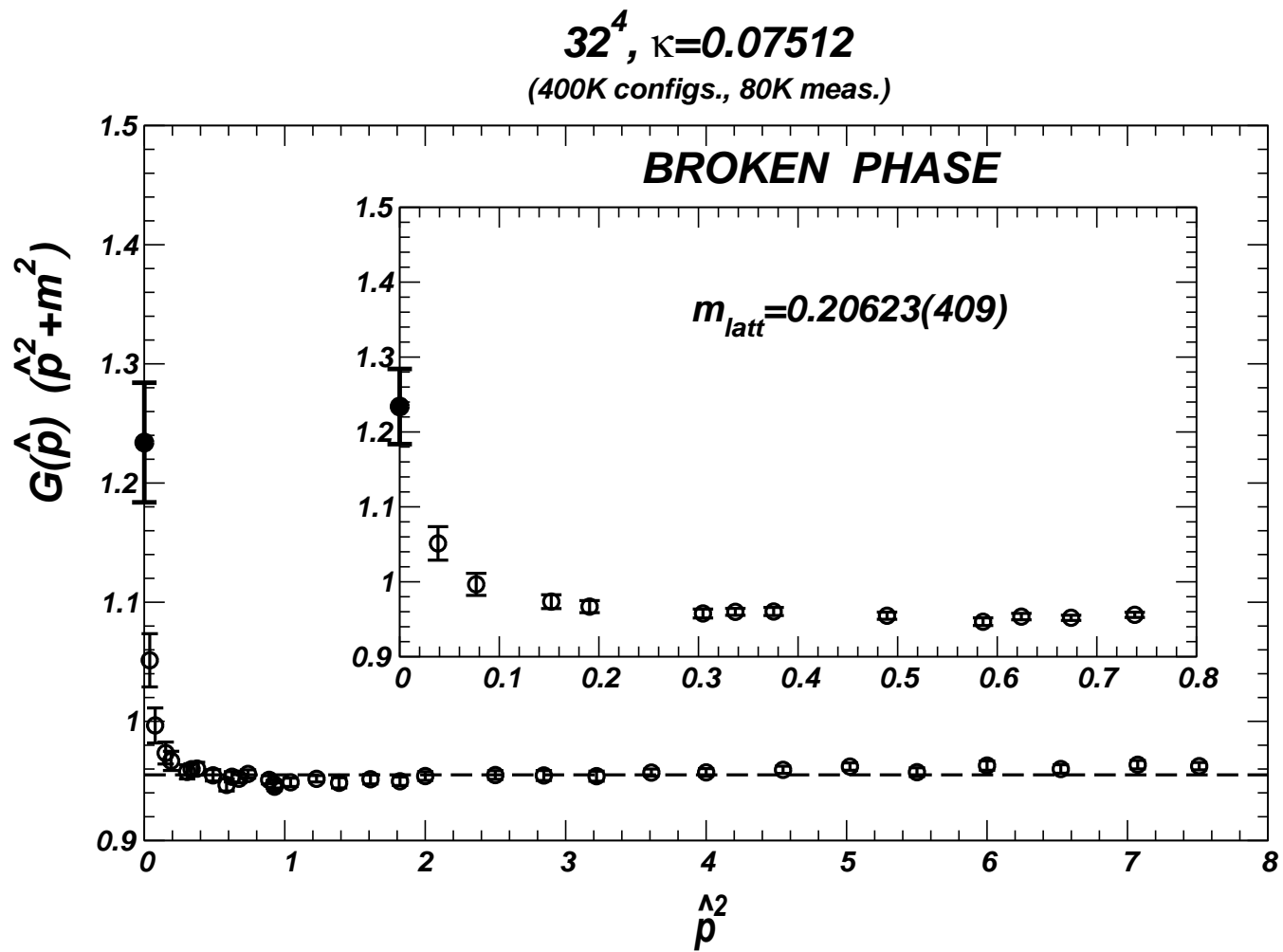


FIGURE 4

$32^4, \kappa=0.07504$
(500K configs., 100K meas.)

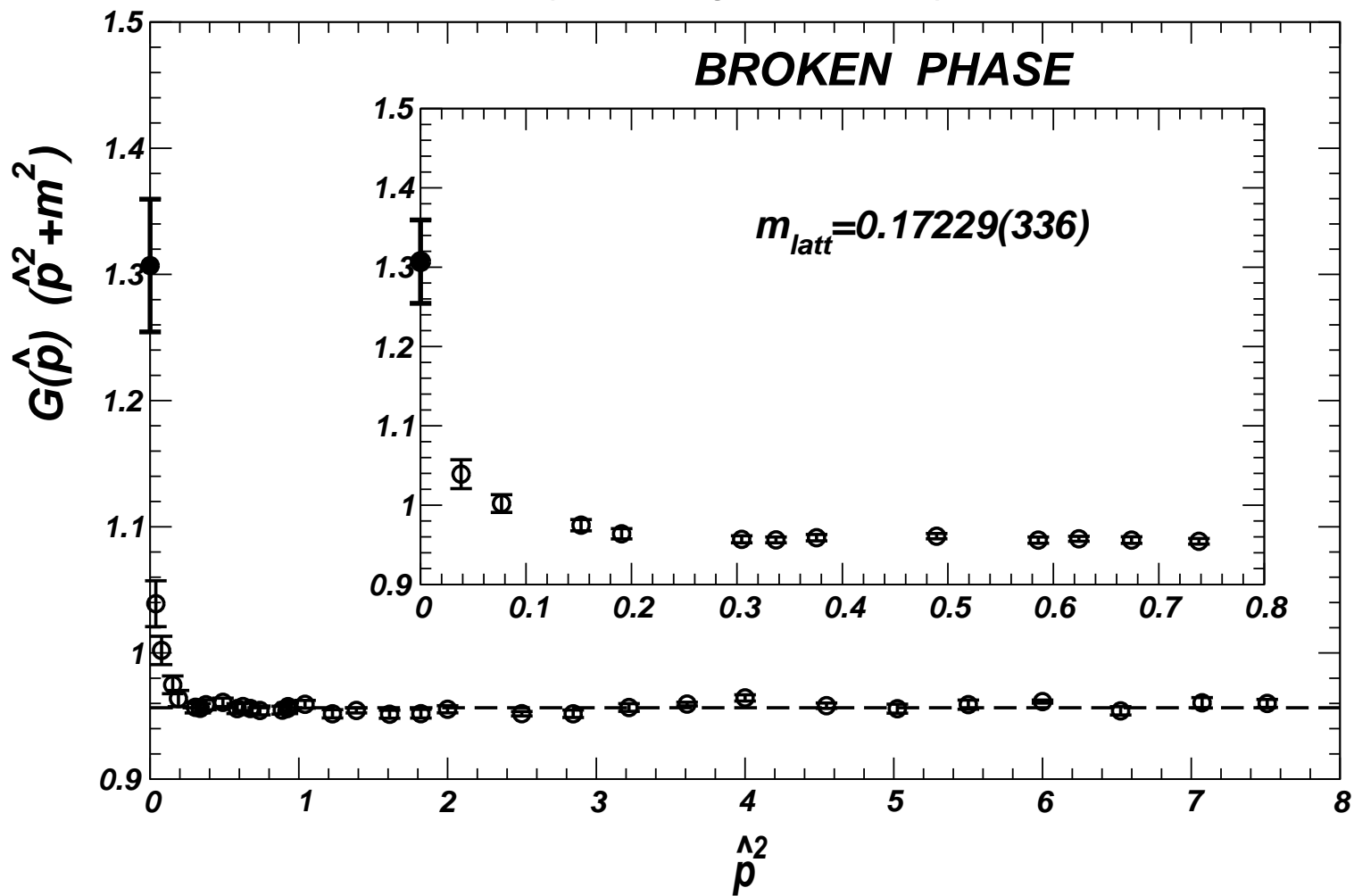


FIGURE 5

FIGURE 6

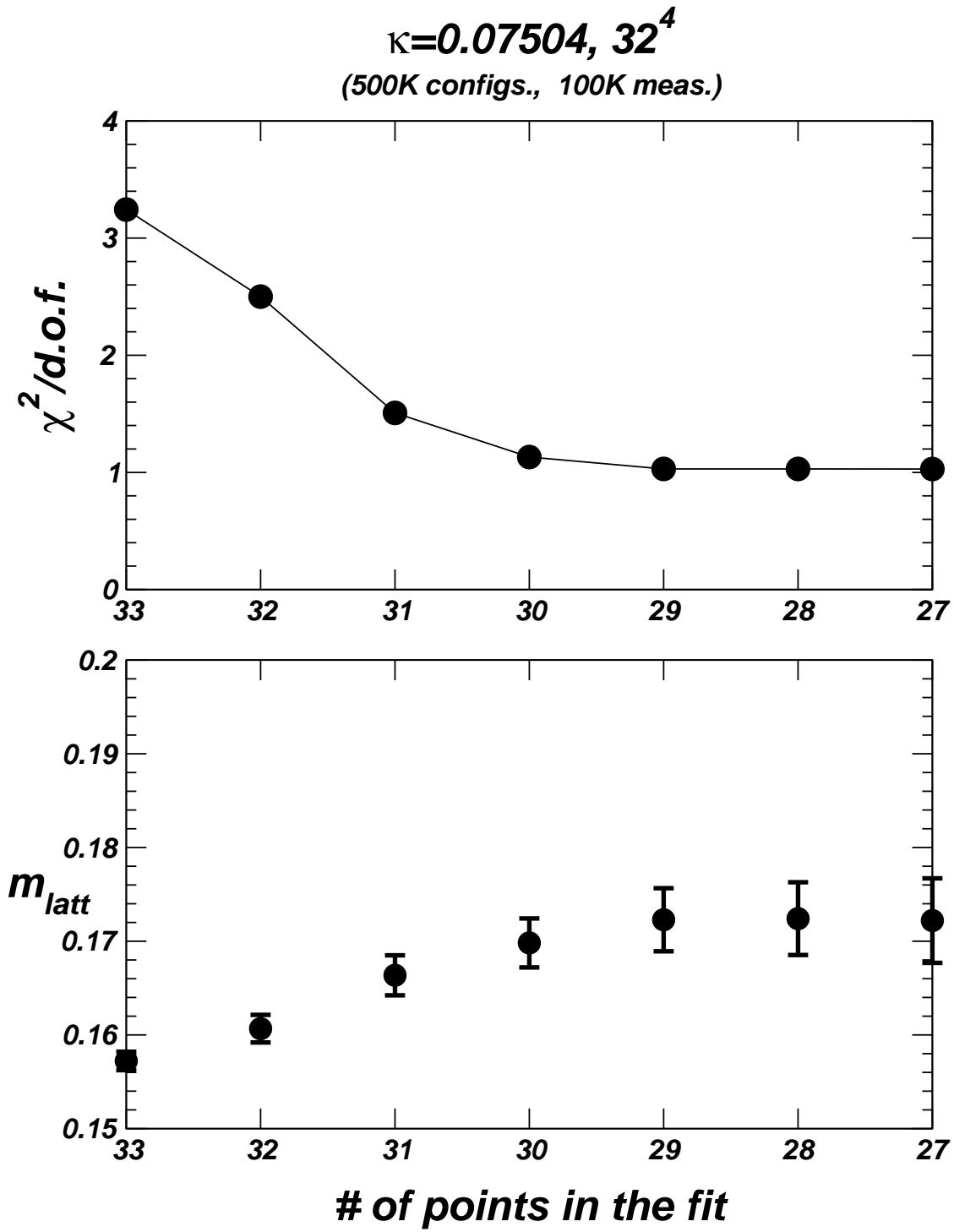
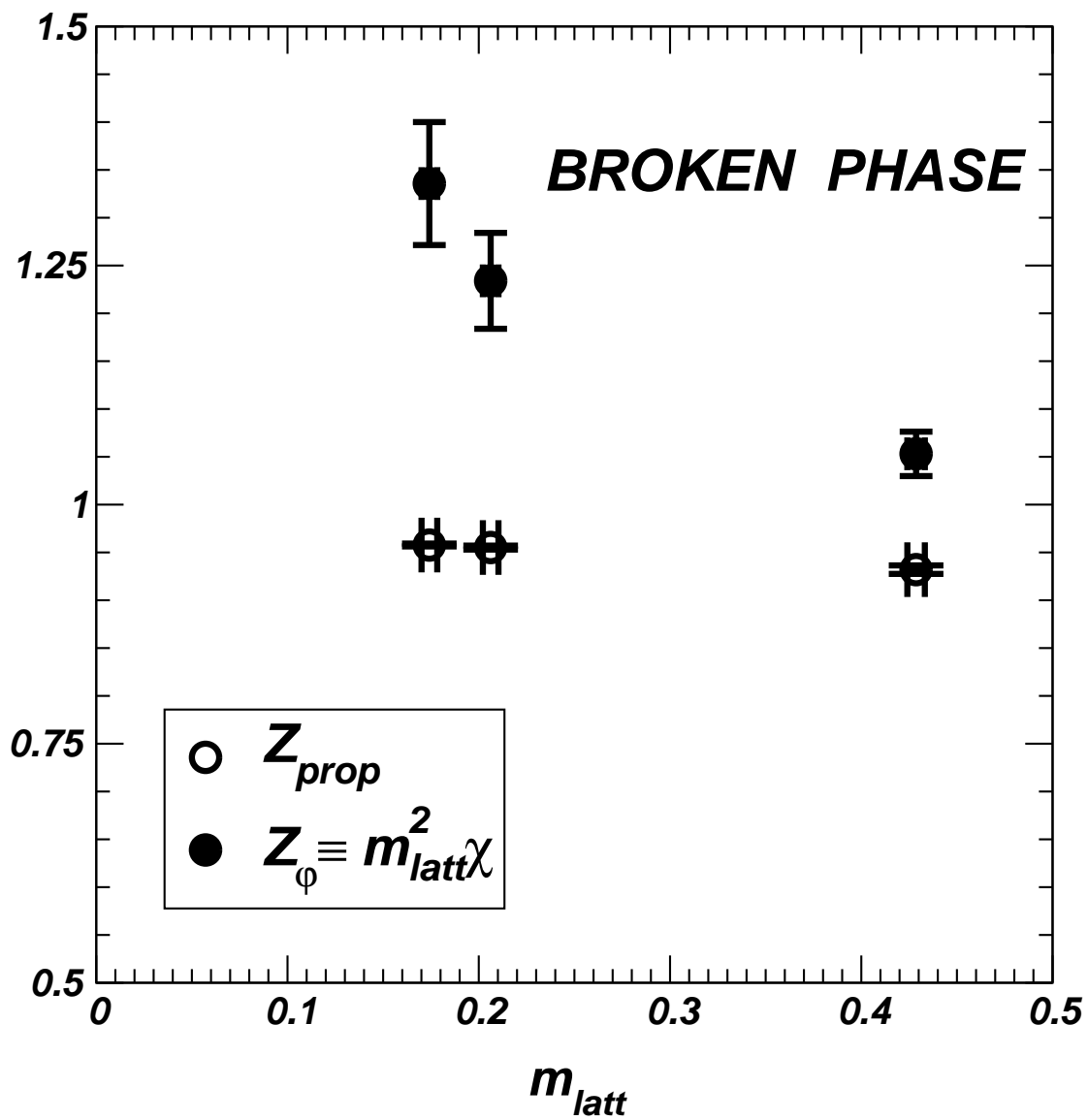


FIGURE 7



$\lambda\phi^4$ Ising model (20^4 lattice)
(230K configs. , 46K meas.)

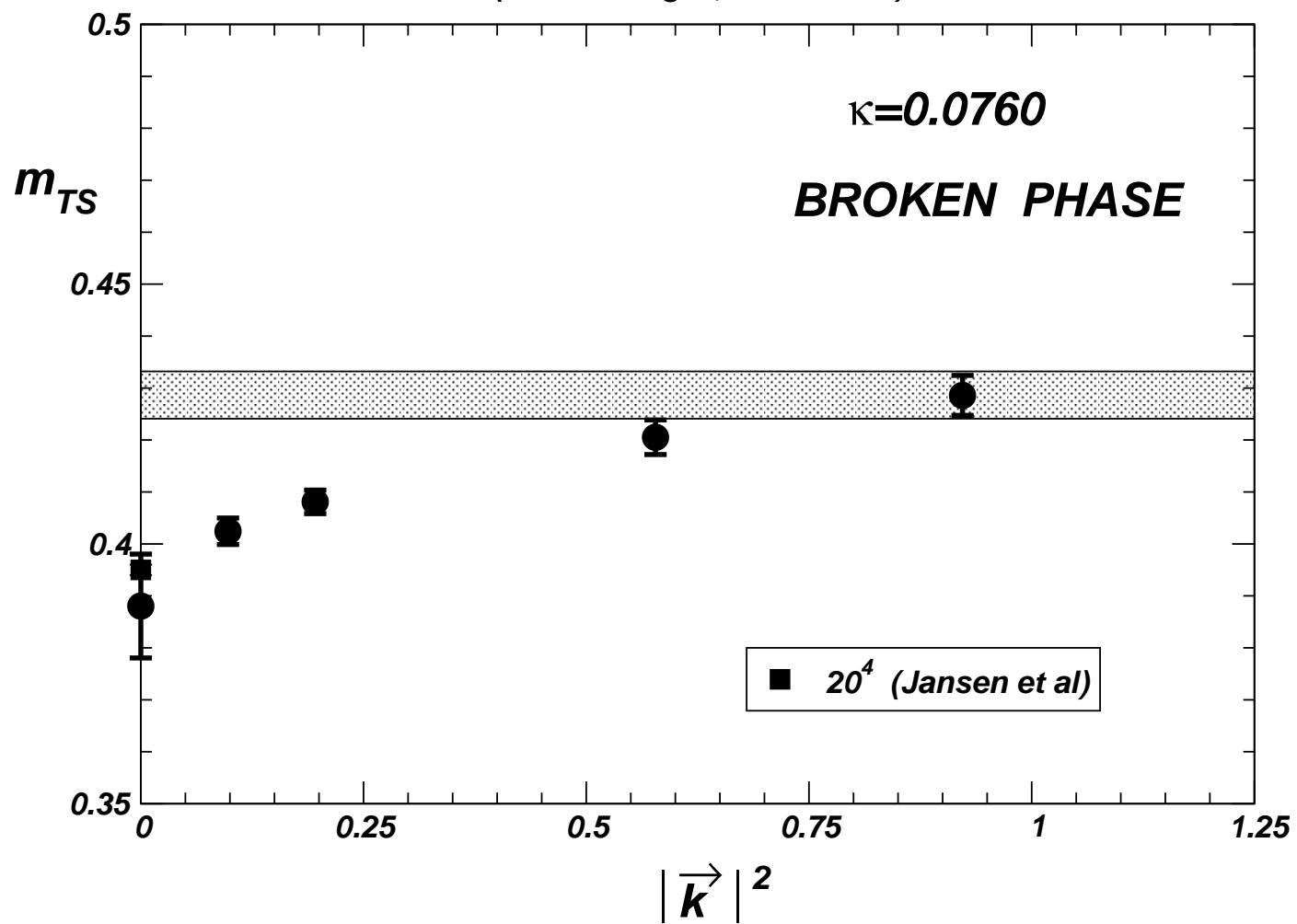


FIGURE 8

FIGURE 9

